



On the Brownian motion of a colloid trapped in optical tweezers: Experiments and simulations

D. Pérez-Guerrero,^{1,a)} B. Morales-Cruzado,^{2,b)} G. I. Guerrero-García,^{3,c)} and E. Sarmiento-Gómez^{4,d)}

¹*Instituto de Física “Manuel Sandoval Vallarta”, Universidad Autónoma de San Luis Potosí, Alvaro Obregón 64, 78000 San Luis Potosí, México*

²*CONAHCYT-Facultad de Ingeniería, Universidad Autónoma de San Luis Potosí, Alvaro Obregón 64, 78000 San Luis Potosí, México*

³*Facultad de Ciencias de la Universidad Autónoma de San Luis Potosí, Av. Chapultepec 1570, Privadas del Pedregal, 78295 San Luis Potosí, México*

⁴*Departamento de Ingeniería Física, División de Ciencias e Ingenierías, Universidad de Guanajuato, México*

(Received 4 November 2021; accepted 29 January 2024)

The trapping potential induced by the interaction of a highly focused laser light with a spherical dielectric particle can be accurately approximated by a parabolic potential. In this work, we revisit experimental and numerical methodologies used to characterize the Brownian motion of a colloidal particle under the influence of a simple harmonic potential produced by optical tweezers. A classic Brownian dynamics simulation is used to model the experimental results, focusing on statistical properties that can be measured by direct visualization of the system using videomicroscopy. This work represents a useful insight into the underlying physics behind the optical tweezers technique, also giving guidelines regarding programming protocols and experimental analysis methodologies, that may be of help for students working with such techniques, as well as for professors teaching undergraduate advanced optics courses. © 2024 Published under an exclusive license by American Association of Physics Teachers.

<https://doi.org/10.1119/5.0077571>

I. INTRODUCTION

A colloidal suspension is formed by a dispersed phase, usually of nanometric or micrometric solid particles, in continuous liquid media. Dispersed particles, also referred to as colloids, should be larger than the ions and small molecules present in the liquid solution, but small enough to be influenced by their interaction with the solvent, thus presenting thermal motion, also called Brownian motion.¹ Brownian motion was first observed by Robert Brown and meticulously characterized by Jean-Baptiste Perrin, finding a null mean displacement as well as the prediction of a mean squared displacement (MSD) that grows linearly in time.^{2,3} Numerical computer simulations are a powerful tool to describe and model Brownian motion. One of the most widely used techniques is Brownian dynamics (BD) simulations.⁴ Experimentally, videomicroscopy is one of the most popularly used tools to observe and study Brownian motion.⁵ In this technique, an optical microscope is used to visualize colloidal particles in a bright field configuration, and tracking routines are used to extract dynamic and static information.

A dielectric, i.e., non-absorbing, colloidal particle interacting with a highly focused laser beam can be modeled as a Brownian particle interacting with a parabolic potential, at least within a short range from the focus of the laser. The colloidal particle is then submitted to the thermal noise due to its interaction with the solvent molecules and to an equivalent force produced by the parabolic potential, the so-called Brownian harmonic oscillator.⁶ This constitutes the working principle of the optical tweezers technique, which has enabled single-molecule experiments in biological systems with great spatial accuracy. The relevance of optical tweezers was recently recognized when Arthur Ashkin was awarded the 2018 Physics Nobel Prize in Physics for the invention of this technique. Understanding the principles

behind optical tweezers is required in a wide variety of undergraduate and graduate programs, particularly in biophysics and related fields. However, the literature discussing both the typical experimental and numerical simulation methods that are used in the field at the undergraduate level is somewhat limited.^{7–9} Moreover, experimental implementations of optical tweezers are nowadays available as modular systems (see, for example, Ref. 10). They are easy to assemble and use and are typically designed as add-on instruments for commercial microscopes.

In this work, we revisit some of the main statistical properties of the Brownian motion of a colloidal particle interacting with a parabolic potential. We also describe an experiment to monitor the motion of a dielectric particle trapped by optical tweezers via videomicroscopy. The present work is divided as follows: in Sec. II, a brief introduction to the main properties of the Brownian motion is presented, along with a general discussion of several relevant observable properties. In Sec. III, experimental and simulation methods are outlined, including sample preparation, tracking, and trajectory analysis. The basic equations and pseudo-codes of the BD simulations we have performed are discussed, and the main components of a typical optical tweezers set-up are presented. Section IV shows the results and the comparison between experiments and numerical simulations. Our main aim is to provide a concise and helpful guide for undergraduate and graduate students interested in understanding and using optical tweezers.

II. BROWNIAN MOTION

Numerous theoretical descriptions of Brownian motion have been proposed since the last century,^{6,11,12} many of them showing a good agreement with experimental observations. Despite all these theoretical advances on the topic,

there are still several significant problems that are far from being fully solved, such as the full description of the hydrodynamic interactions among colloidal particles,¹ the effect of external potentials on the colloidal suspension,^{13,14} or non-equilibrium conditions.^{15–17}

The first theoretical framework we revisit is an equation of motion known as the Langevin equation.¹⁸ The underlying basis of this framework is the separation of the net force exerted by the solvent on a particle as the sum of a random stochastic force (memoryless force) and a friction force (shape- and liquid viscosity-dependent). Although the random force cannot be fully described, some statistical properties can be derived, and thus, the Langevin equation becomes a stochastic equation of motion, i.e., an equation for which only noise-averaged quantities can be computed. In the following, we will restrict ourselves to the one-dimensional Langevin equation

$$m \frac{dv}{dt} = -\gamma v + f_R(t) + f_{ext}, \quad (1)$$

where m is the mass of the particle, $-\gamma v$ represents the velocity-dependent friction force with friction coefficient γ , $f_R(t)$ is the random force due to solvent collisions, and f_{ext} corresponds to the sum of all other external forces. The external force can be associated, for instance, with the external field produced by optical tweezers or with the net force that the particle experiences due to the presence of other particles in non-dilute systems. The formalism for solving the Langevin equation is usually limited to times larger than the inertial time, m/γ , for which diffusive motion is always found. The inertial time for micrometer particles in an aqueous solution is typically about 100 ns.¹⁹ The friction and the random forces actually come from the same origin, namely, the random impacts of surrounding solvent molecules on the tracer particle, but they, respectively, represent the force that depends on the particle's velocity and the force that is independent of it. Note that the fluctuation–dissipation theorem is a direct consequence of the relationship between the friction and random forces.²⁰

Given that it is impractical to calculate the forces due to collisions between the colloidal particle and $N \sim 10^{23}$ solvent particles, $f_R(t)$ is usually only defined by its statistical features. For spherical colloidal particles of radius r with no-slip boundary conditions for the flow field, one gets

$$\langle f_R(t) \rangle = 0, \quad (2)$$

$$\langle f_R(t) f_R(t') \rangle = \frac{6\pi\eta r k_B T}{m} \delta(t - t'), \quad (3)$$

where $\langle \rangle$ denotes an ensemble average. Notice that Eq. (3) indicates that there is no correlation between the random forces at two different times t and t' . The main property we are interested in is the one-dimensional mean squared displacement, MSD, defined as $\langle \Delta x^2(t) \rangle \equiv \langle (x(t) - x(0))^2 \rangle$. In the absence of external forces, the MSD predicted by the solution of the Langevin equation exhibits, at short times, a so-called ballistic regime, i.e., a regime where the MSD $\propto t^2$. More importantly, at longer times which correspond to the regime usually accessible experimentally, the MSD grows linearly with time,

$$\langle \Delta x^2(t) \rangle = 2Dt, \quad (4)$$

where D is the diffusion coefficient that depends on temperature and on the friction coefficient γ as $D = k_B T / \gamma$. (This relation is also known as the Stokes–Einstein equation.)¹ For a spherical particle of radius r in a solvent at temperature T and viscosity η , the diffusion coefficient can be expressed as $D = k_B T / 6\pi\eta r$.

Optical tweezers create an external parabolic potential due to the interaction of a Gaussian laser beam with the spherical particle, so that the effective trapping force is usually modelled as $f_{ext} \approx -kx$,⁸ where k is the spring constant or optical stiffness and depends on the laser's incident power and wavelength, as well as on the size and on refractive index of the particle and the refractive index of the surrounding medium. With such a trapping force, the MSD takes the following form:^{6,21}

$$\langle \Delta x^2(t) \rangle = \frac{2k_B T}{k} \left[1 - \exp\left(-\frac{kt}{\gamma}\right) \right]. \quad (5)$$

Equation (5) presents two time regimes: at short times, $t \ll \gamma/k$, the MSD grows linearly and the particle is free to randomly move around $x=0$, and one recovers Eq. (4). At long times, $t \gg \gamma/k$, the MSD is time-independent and equal to the constant value $2k_B T/k$: the optical tweezers create a confinement region from which the particle is unable to escape. The second regime is also used to calibrate the optical tweezers: the spring constant k can be inferred by experimentally determining the MSD and fitting it to Eq. (5).

An alternative formalism to describe the Brownian motion is related to the Fokker–Planck equation first developed by Einstein.^{8,12} This equation describes the evolution of the probability density $\rho(x, t)$ of finding a particle at a position x at time t if the particle was found at $x=0$ at $t=0$. In the simplest case where the diffusion coefficient is independent of time and space and in the absence of external forces, the Fokker–Planck equation takes the form

$$\frac{\partial \rho(x, t)}{\partial t} = D \frac{\partial^2 \rho(x, t)}{\partial x^2}. \quad (6)$$

As in this formalism the particle's inertia is neglected, and the associated velocity does not display a ballistic regime.²²

By using the initial condition $\rho(x, t=0) = \delta(x)$, the solution to Eq. (6) is expressed as

$$\rho(x, t) = \frac{1}{\sqrt{4\pi Dt}} \exp\left(-\frac{x^2}{4Dt}\right), \quad (7)$$

and thus, the particle probability density evolves as a time-dependent Gaussian function. As it is shown below, the probability density can be estimated experimentally from displacement histograms.²³ In this case, the MSD is calculated as the second moment of the probability density, giving the same result as the Langevin description for $t \gg \gamma/k$. However, both the Fokker–Planck and the Langevin equations are complex to solve for an arbitrary external force, and thus, a new methodology is required.

To circumvent this difficulty, Ermak proposed in 1975²⁴ an important algorithm for solving ordinary differential equations, including the classical diffusion equation that describes the one-dimensional stochastic motion of a particle in a molecular solvent, which is the so-called Smoluchowski equation,

$$\frac{\partial P_X(x, t|x_0, t_0)}{\partial t} = -\frac{1}{\gamma} \frac{\partial}{\partial x} (f_{ext}(x) P_X(x, t|x_0, t_0)) + D \frac{\partial^2 P_X(x, t|x_0, t_0)}{\partial x^2}, \quad (8)$$

where $f_{ext}(x)$ represents the net external force acting on the particle and $P_X(x, t|x_0, t_0)$ represents the probability density function of finding a particle at the position x at time t if the particle was initially located at x_0 at time t_0 . The Smoluchowski equation (8) is equivalent to the Langevin equation (1) if the magnitude of the frictional force γv is much larger than the inertia $m(dv/dt)$.²⁵

Similar to the Fokker–Planck equation, Eq. (8) needs an explicit functional form of the external force to be solved. However, the methodology proposed by Ermak is fundamentally different from analytically solving such equation, being an iterative method. In a Brownian dynamics simulation, the position of the particle at the time $t + dt$ is calculated from the previous position at time t ,²⁴

$$x(t + dt) = x(t) + D \frac{f_{ext}(x(t))}{k_B T} dt + \sqrt{2Ddt} G(t), \quad (9)$$

where the first term corresponds to the position of the particle at time t , the second one corresponds to the displacement due to the external force, and the last one represents a random displacement, which is normally distributed with a zero mean and has a variance $2Ddt$, where $G(t)$ corresponds to a Gaussian random variable.

Another statistical property of interest is the time-independent probability density

$$\rho(x) = \int \rho(x, t) dt, \quad (10)$$

which gives the probability of finding a particle at a certain position x regardless of the specific time t . At thermodynamic equilibrium, and considering sufficient long and independent sampling of the positions, the time-independent probability density follows the Boltzmann distribution,

$$\rho(x) \propto \exp\left(-\frac{U_{ext}(x)}{k_B T}\right), \quad (11)$$

where U_{ext} is the external potential, defined as $f_{ext} = -dU_{ext}/dx$. Thus, the time-independent probability density can be written as a Gaussian function dependent on the spring constant k ,

$$\rho(x) = \sqrt{\frac{k}{2\pi k_B T}} \exp\left(-\frac{kx^2}{2k_B T}\right). \quad (12)$$

The Boltzmann distribution reflects the fact that a thermal system in equilibrium is more likely to be found in the minimum of the potential. Again, such a distribution can be calculated from the position histogram.

III. METHODS

A. Videomicroscopy and mean squared displacement calculation

The Brownian particles used in this work have been chosen to be of the order of a micrometer in size so that they can

be visualized using classic optical elements. The drag force exerted by the solvent can also be calculated using the Stokes relation. Moreover, these particles are commercially available in water solution and display minimal variation in size.

For the determination of the diffusion coefficient, a sample is prepared from the original stock solution (Fluka spherical polystyrene particles of $2.8 \mu\text{m}$ in diameter in a water solution at 0.1 weight/weight concentration) to reach an area fraction (the ratio of the transverse area of all particles over the total area) of 0.01 to avoid particle interaction. Particles smaller than $1 \mu\text{m}$ can be used but would probably be difficult to resolve optically, whereas larger particles may have a reduced Brownian motion, making the calibration protocol complex. The sample is then mixed with a dilute (about 0.001 in area fraction) solution of larger particles (Fluka spherical polystyrene particles of $4.0 \mu\text{m}$ in diameter). The solution is agitated to avoid sedimentation, and a volume of about $10 \mu\text{l}$ of the mixture is placed on top of a glass plate, covered with a No. 1 cover glass, gently pressed down and sealed with fast curing epoxy adhesive liquid to avoid drift caused by air flow. Prior to assembly, the glass plate and cover glass are cleaned using Hellmanex III cleaning solution in ultrasonic bath, washed against ultra-pure water ($18 \Omega\text{M}/\text{cm}$) several times and dried in a vacuum oven at 100°C . These steps are important to ensure that the larger particles serve as spacers to set the thickness between the glass plate and the cover glass, while the small particles are confined to a quasi-2D space, remaining in focus for the total duration of the experiment and facilitating the tracking of the particles. This procedure also helps us to determine the best tracking parameters for further experiments. The sample can be placed on the experimental setup used for optical tweezers, which is detailed below, but it can also be observed in a commercial inverted bright field microscope (Nikon Eclipse Ti-U) using a $20\times$ microscope objective, with the advantage of being able to track the ~ 100 particles that are in the field of view to have a better statistics, as shown in Fig. 1. Recording at 10 frames per second in these conditions gives a reliable mean squared displacement after 2000 s, as is shown below.

Samples for optical trapping are prepared similarly but with a lower concentration of particles to reduce the probability of another particle interacting with the trapped particle and using a high aperture microscope objective.

Tracking algorithms^{23,26} can be used to calculate a wide variety of statistical properties. Tracking methodologies usually start from a series of images obtained from a camera software, and, using the well-known method proposed by Crocker and Grier, the centroid of a particle (usually brighter than its surroundings) is tracked.²³ Trackpy, an open toolkit in Python that implements the Crocker and Grier algorithm, was used here to track the position of colloidal particles experimentally, achieving sub-pixel accuracy.⁴⁰ The accuracy depends on the microscope, but, in our case, gives a typical resolution of 100 nm . Trackpy is also able to compute the drift of the particles (caused, for example, by a tilt of the sample) and to subtract such a drift from the trajectories. In most cases, drift affects the long-term dynamics, and thus, a reliable analysis at such times requires removing the drift even if it is found to be small. The outcome of the Trackpy algorithm is the trajectory of the particles, i.e., a time series of the position of the particle at each frame x_j separated by a

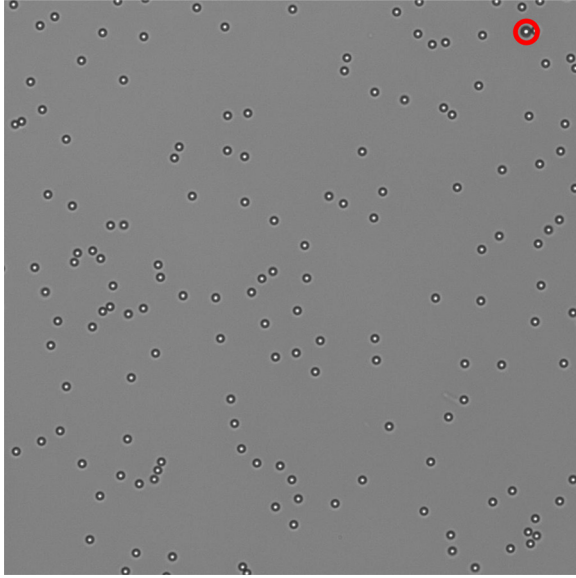


Fig. 1. Representative image of a dilute colloidal suspension, as seen by bright field microscopy using a 20 \times microscope objective. A time series of such images is used to determine the diffusion coefficient of the colloids as well as the parameters to be used by the Brownian dynamics simulation. One of the larger particles, used as spacers, can be seen in the right top corner (inside the red circle).

time $dt = 1/\text{fps}$, where fps is the number of frames per second acquired by the camera.

The MSD is calculated by computing the squared displacement at different times and performing an ensemble average, i.e., averaging over all particles on the field of view for the free diffusion experiment. In addition, a time average can be performed to improve precision on the MSD if the system is stationary, i.e., if the statistical properties do not change in time, then the MSD for a single particle for a particular time interval can be calculated starting at any of the observed times t_i . Denoting the time between frames as dt and the time interval $t = j \times dt$, where j must be an integer, the MSD of a trajectory of size n for the time interval t can be calculated as

$$\langle \Delta x^2(t = j \times dt) \rangle = \frac{1}{n-j} \sum_{i=1}^{n-j} (x(t_i + jdt) - x(t_i))^2. \quad (13)$$

This average would correspond to the ensemble average if n is large enough for the particle to sample the whole phase space. This quantity can then be averaged over the entire ensemble of particles. Note that it is possible for time-averaging and ensemble averaging to give different results,^{27,28} but we did not observe this effect. In Eq. (13), the number of averaged points decreases as t increases, ranging from $n - 1$ for the first lag time to 1 for $t = n \times dt$. The number of averaged data points is a measure of the statistical reliability at a particular time, and thus the uncertainty increases as the lag time increases. Particle averaging contributes to improving the statistics, especially at long times. For the calculations made in this contribution, the MSD is found to be statistically reliable for lag times smaller by a factor of 10 than $n \times dt$ for a single trapped particle.

Figure 2 shows representative individual and time-averaged mean squared displacements for the case of free particles (grey lines), along with the calculated ensemble-

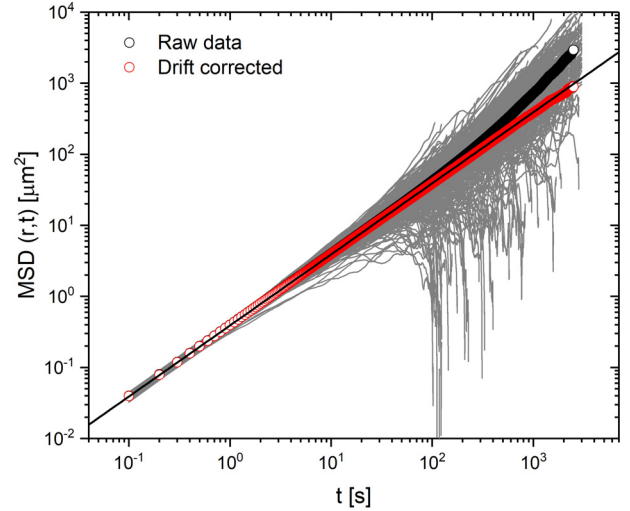


Fig. 2. Individual non-corrected mean squared displacements of colloidal particles (diameter 2.8 μm) in water, that are confined between two glass plates (gray lines). Symbols show the ensemble-averaged two-dimensional MSD without (black circles) and with (red circles) drift correction.

averaged MSD from the raw trajectories, i.e., without removing the drift (black circles). As can be seen, slightly different diffusion coefficients are found for each one of the trajectories at short times, due to small variations in the position of the particles but also to statistical deviations. At large lag times, larger deviations are observed due to statistical uncertainty produced by the truncation of the sampled trajectories that occurs when particles leave the image volume. Furthermore, the effect of the drift on the MSD can be observed on an individual particle's MSD, as, at long time, the displacements are larger than expected from diffusion. More importantly, the ensemble-averaged MSD also presents this feature, deviating from linearity at times larger than 100 s. Removing the drift using Trackpy routines gives an ensemble averaged MSD that remains linear up to the maximum time where the MSD was calculated (red circles), in this case 3000 s, highlighting the importance of subtracting the drift from the trajectories. The diffusion coefficient obtained from a linear fit to the drift-corrected MSD is $D = 0.09587 \pm 0.00001 \mu\text{m}^2/\text{s}$, which deviates from the Stokes–Einstein value, namely, $0.1227 \mu\text{m}^2/\text{s}$, mostly because of the hydrodynamic interaction of the particles with the glass plates that hinders their motion.

B. Optical tweezers setup

In an experimental realization of the Brownian harmonic oscillator, the trapping force exerted on the particle by a laser beam comes from the change of momentum of the incident photons scattered by the particle due to the change in refractive index at the colloid–solvent interface. As the photon momentum is proportional to its frequency, the refraction-induced force is negligible in most cases. However, this force may be important for high intensity light sources (such as laser beams) and micro-sized dielectric particles. Such a trapping phenomenon was successfully implemented experimentally by Arthur Ashkin in the 1970s. He first succeeded in levitating a particle using a laser beam shining on it from below,²⁹ before trapping a smaller Brownian particle in 3D with two counter-propagating beams,³⁰ and finally inducing the same 3D trapping with a single highly focused laser

beam.³¹ This method is known as an optical tweezer and has important applications in several scientific fields.^{32–34} The force exerted on a particle trapped by typical optical tweezers is of the order of piconewtons for visible light in the milliwatt power range.⁸ The magnitude of such a trapping force is comparable to the drag force of micrometer particles in microfluidic devices or to the interaction forces among colloidal particles.³⁵

A schematic of the experimental setup used to trap particles in a laser-induced parabolic potential is shown in Fig. 3, along with an image of the actual apparatus. It is composed of image formation elements and optical trapping parts. In our setup, we trap a single particle at any given time. The trapping laser provides a beam of power up to 2 W, as measured at the exit of the laser, at a wavelength of 532 nm (Opus532, Laser Quantum). A key element in both the trapping and the image formation optical components is the use of a 100×, N.A. 1.35, microscope objective (Nikon E plan 100×, infinite-corrected), capable of focusing laser light on a very small region where the trapping occurs. It also produces a magnified image of the trapped particle. A Halogen lamp (QTH10, Thorlabs) provides a homogeneous illumination of the sample, using an iris diaphragm to control light

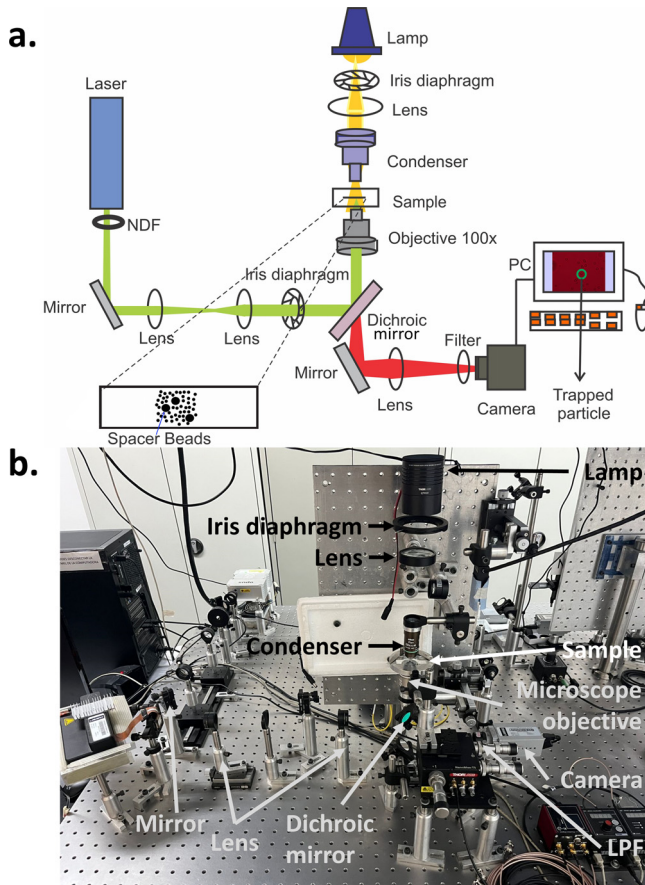


Fig. 3. (a) Schematic representation of the experimental set-up for optical trapping. Coherent light from a 532 nm laser is expanded using a telescope and redirected to a high numerical aperture microscope objective using a dichroic mirror with a cut-off wavelength of 605 nm. The beam is focused on the focal plane of the microscope objective, where the sample is located, and optical trapping is achieved. Light from a white source is directed onto the sample using a single lens and a condenser. The light coming out of the microscope objective is taken out to a camera by a single lens. A long pass filter (LPF) filters laser light that may be reflected back to the camera. (b) Picture of the experimental set-up.

intensity and two refractive elements (a single lens and a condenser). An additional lens takes the image formed by the microscope objective to the camera plane. A dichroic mirror (DMLP605, Thorlabs) joins both sets of elements, by reflecting the trapping laser beam to the 100× microscope objective and allowing the formation of the image in the camera (PL-B776F, Pixelink) using the filtered light of the lamp (in the red part of the visible spectra in this case). Stable trapping is achieved by increasing the laser beam size to slightly overfill the back aperture of the microscope objective. To this end, a telescope is used to increase the laser beam’s diameter by a factor of 6.⁷ As the particle is highly confined in the central part of the image, the region of space captured by the camera can be reduced so as to be able to increase the number of frames per second. In this particular case, 500 fps can be reached using a 256 × 256-pixel region. The camera’s spatial resolution limits the higher laser power that can be used in the experimental setup as increasing laser power reduces the amplitude of the particle’s motion. In our case, the maximum laser power is about 20 mW. At room temperature, simulations based on the absorption coefficients of both water and the particle show that this power should not affect the solution’s temperature in any significant manner.

C. Brownian dynamics simulation

Brownian dynamics simulations are a powerful numerical technique that allows us to delve into the study of the dynamics and statistical properties of a particle system under the influence of an external field. Once the BD simulations are calibrated using preliminary diffusion constant experiments and long timescales MSD as explained below, they can be used to explore values of the parameters (strength of the laser, particle size, etc.) that it would be either impractical or too time-consuming to test experimentally. In the Brownian dynamics (BD) approach, the Langevin equation is solved by simulating the random motion of particles originating from the thermal agitation produced by the host solvent. The BD formalism is very well developed and can include hydrodynamic interactions among particles,⁴ as well as forces produced by external fields such as electric³⁶ or magnetic forces,³⁷ confinement, and gravitational effects,³⁸ among others.

In this study, we have performed Brownian dynamics simulations of a particle under the influence of a parabolic potential with the following form:

$$U(x) = \frac{1}{2}kx^2, \quad (14)$$

where k is the spring constant associated with the potential which is experimentally determined using the long time-scales MSD (Eq. (4)). Once the external potential is set, the trajectory of a particle can be simulated using the solution developed by Ermak (9) outlined in Sec. II.

The confining potential of the laser is counter-balanced by the kinetic energy of the particles. In the BD simulations, we introduce the thermal energy

$$U_0 = \alpha k_B T, \quad (15)$$

where α quantifies the thermal energy in units of $k_B T$. To determine α , which is an input of the BD simulations, one can, for instance, postulate that the thermal energy is equal

to the typical potential energy of the trapped particle when it has moved one diameter a away from its equilibrium position,

$$k = \frac{2\alpha k_B T}{a^2}. \quad (16)$$

Such an assumption allows to have a dimensionless energy parameter for the simulations. Since it is constrained by the long timescales MSD (Eq. (4)), the exact model relating k to $k_B T$ does not affect the results of the experiments.

Once the trajectories of the particles are simulated using the BD algorithm, it is possible to estimate some important static and dynamic properties, such as the MSD or the probability density function, as it is done experimentally by using the recorded trajectories.

IV. RESULTS OF BROWNIAN MOTION IN A PARABOLIC POTENTIAL

For particles trapped in optical tweezers, in contrast to the case of free diffusion, we do not need to confine the colloidal particles between two glass plates to observe a 2D motion. This is because the trapping force prevents any sedimentation, thus confining the particle's motion to a plane. This also allows to keep the trapped particle in focus during the whole experiment. Note that the diffusion coefficient depends on the confinement, so that special care should be taken if the diffusion and the optical tweezers experiments are not performed using the same confinement, whether induced by glass plates or by the optical tweezers.

In order to compare the dynamics of a trapped colloidal particle with the Brownian dynamics simulation, some parameters must be determined first, mainly the diffusion coefficient D , which can be determined as indicated in Sec. III A, and the spring constant k associated with the optical stiffness (that can be given in terms of α , as discussed above). As k mainly depends on the laser power and the particle's size, we can be tempted to determine this parameter once for a given laser power (fitting the experimental MSD to Eq. (5)) and use this value for further experiments. However, small variations in either the trap's position or the sample preparation influence the effective trapping power. Thus, *in situ* calibration is always preferred.

We measured the time-averaged MSD of a $1.0 \mu\text{m}$ diameter particle confined by the laser at powers ranging from 4 to 18 mW. The duration of each experiment was 1000 s, giving 10 000 frames recorded at 10 fps, enough to get reliable statistical information. The experimental MSD is shown in Fig. 4 (black dots) for a laser power of 6 mW. From the fit to Eq. (5), the value of the spring constant has been extracted: $k = 1.3886 \text{ pN}/\mu\text{m}$ for this particular case. The value of D has been extracted from the analysis of Fig. 2 (for $2.8 \mu\text{m}$ particles) as explained above and has been renormalized for the particle size via the Stokes–Einstein relation. The values of k and D have been used as inputs for the BD simulations for all laser powers experimentally studied. The simulations have been run with a time step $dt = 1 \times 10^{-6} \text{ s}$, so that the first observed experimental point is three decades in time later than the first simulation time. In Fig. 4, for clarity, the MSDs extracted from the BD simulations are shown only in the range where experimental data are accessible. This form of the MSD is observed for all laser powers: at short times, the MSD grows linearly with time, indicating free diffusion,

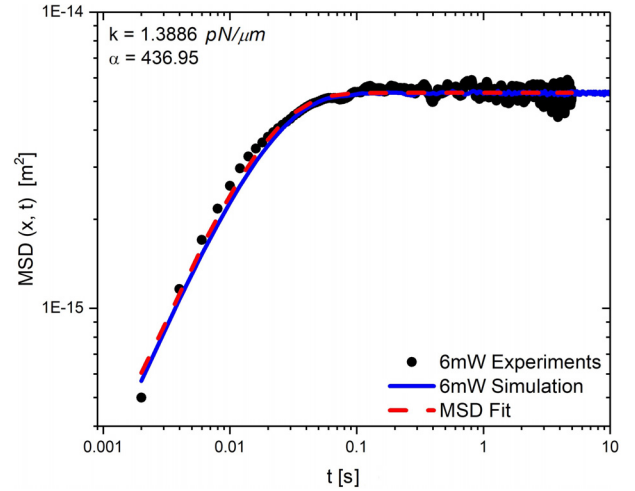


Fig. 4. One dimensional mean square displacement of Brownian particles of diameter $= 1.0 \mu\text{m}$ trapped by optical tweezers at a laser power of 6 mW (black circles) and comparison with numerical Brownian dynamics simulations (blue line). The diffusion coefficient in the absence of optical tweezers was estimated using the MSD shown in Fig. 2, whereas the spring constant was obtained as a fit to Eq. (5) indicated as a red dashed line.

while at longer times, the MSD develops a plateau due to the confinement of the particle by the optical tweezers. Thus, the long time regime depends on the laser power used for optical trapping.

Before analyzing time-dependent properties, it is interesting to analyze the behavior of the equilibrium, or time-independent, probability density function $\rho(x)$, which gives the probability per unit length of finding the particle around the position x , averaged over time. As stated above, at thermodynamic equilibrium, the time-independent probability function should follow a Boltzmann distribution. As the particle is trapped in a potential of the form $U(x) = \frac{1}{2}kx^2$, the expected Boltzmann distribution should be Gaussian as shown in Eq. (12). A Gaussian profile of the time-independent probability function $\rho(x)$ is indeed observed in the experimental results and in the numerical BD simulations (see Fig. 5) not only for the laser power shown, but for all laser powers explored experimentally. The extent of the probability function $\rho(x)$ can also be understood as the size of the trapping potential induced by the interaction of the laser beam with the particle and thus reduces in size when increasing laser power. In the following, we explore the properties of the probability density function at different laser powers, where some of the features explained above are better explored.

When the laser power increases, the spring constant k associated with the optical tweezers increases and the spatial confinement of the particle is expected to increase. As a result, a sharpening of the time-independent probability distribution is observed, and the width of Gaussian profile reduces according to Eq. (12). The increase in the optical stiffness as a function of the laser power P can be characterized by two equilibrium parameters: the maximum height of the time-independent probability density $H_{Max}(P) = \rho(x = 0, P)$ and the width of a Gaussian fit $\sigma(P)$ (and variance $\sigma^2(P)$), which are shown in Figs. 6(a) and 6(b). Similarly as in the previous case, the optical stiffness k has been estimated from experimental data for different laser powers as a fit to Eq. (5) and used to feed the BD simulation. From the

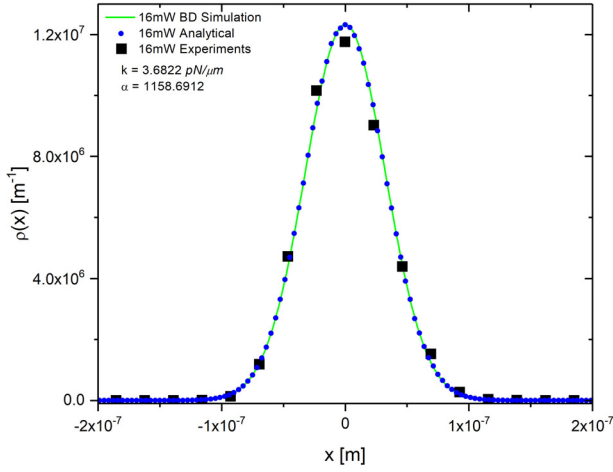


Fig. 5. Time-independent density of probability of finding the trapped particle at the position x . Blue circles represent the experimental data associated with Fig. 4. From calibration methods, the experimental k is calculated, giving $3.68 \text{ pN}/\mu\text{m}$ or equivalently $\alpha = 1158.69$, and it is used as an input parameter in both the numerical BD simulations and the analytical Boltzmann distribution given by Eq. (12), which are shown as a green line and black squares, respectively. The observation time step was set to 0.002 s for the experiment and the BD simulations.

trajectories tracked experimentally and those obtained by the simulation, the time-independent probability distribution is calculated, and the two above-mentioned parameters are estimated. In both instances, simulations and experimental data display a good agreement. This is expected, since, in both cases, the dynamics are almost equivalent (see Fig. 5 for instance), reflecting the correct choice of parameters used in the effective potential associated with the optical tweezers. According to Eq. (12), the variance $\sigma^2(P)$ should inversely depend on the optical stiffness. Figure 6(b) shows that the variance is inversely proportional to the laser power, which implies a linear relation between the laser power and the optical stiffness. This relation is expected, as increasing the laser power is related to an increase in the number of

incident photons, and as each photon contributes similarly to the optical trapping, an increase in the optical stiffness is expected. This finding is also well known and has been reported in the literature.³²

As indicated above, the probability density function $\rho(x, t)$ fully characterizes the dynamical behavior of the Brownian motion of a particle trapped in optical tweezers. In the absence of an external field, that is in pure Brownian motion, the theoretical form of $\rho(x, t)$ is given by Eq. (7), which represents a Gaussian profile with a width that increases with time. Even though such a quantity can be computed at any lag time, we are mainly interested in showing the behavior of $\rho(x, t)$ in three different regimes: at short-times, when the dynamics is diffusive and $\rho(x, t)$ is Gaussian; at long-times, when t is larger than the characteristic trapping time $\gamma/k = (k_B T)/Dk$ (see Eq. (5)) and the MSD clearly displays a plateau; and at the transition time regime between short- and long-times. In Fig. 7, the probability function for our experiments and simulations is shown at four experimental lag times: $\tau = 1, 4, 50$, and 400 , with $\tau = t/(100 \text{ ms})$, at a laser power of 6 mW . At lag time $\tau = 1$, the experimental and BD simulations display a high and narrow peak for $\rho(x, t)$. At long-times (see, e.g., $\tau = 50$ and $\tau = 400$), $\rho(x, t)$ displays a constant height and a stationary Gaussian shape according to experimental results. Interestingly, the BD simulation converges to the same values as the experiments in this regime. At the transition time regime between the short- and long-times (see, e.g., $\tau = 4$), the $\rho(x, t)$ also presents a Gaussian shape.

V. CONCLUSIONS

In this work, we have revisited some of the most important features of a colloidal particle undergoing Brownian motion when interacting with a highly focused laser beam in the visible range. This interaction produces the so-called optical trapping phenomenon, i.e., the contactless manipulation of the particle with a force of the order of pico-Newtons, with huge applications in biology and physics. The experimental implementation of optical tweezers is

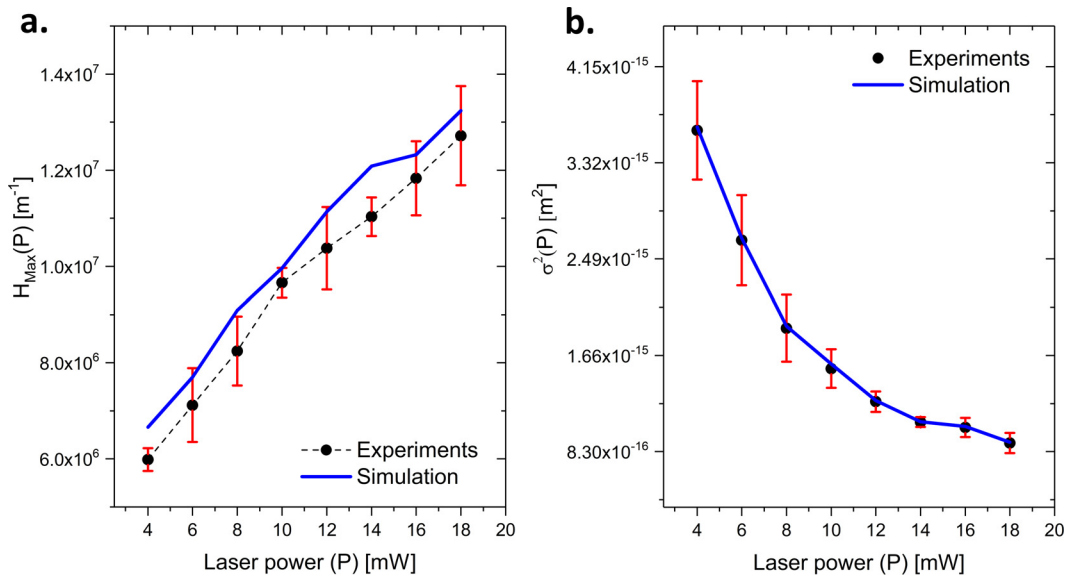


Fig. 6. (a) Maximum time-independent probability density per unit length at $x = 0$. (b) Eidth of the time-independent probability density per unit length for different laser powers. The blue lines and the black circles represent the results obtained from numerical Brownian dynamics simulations and from experiments, respectively.

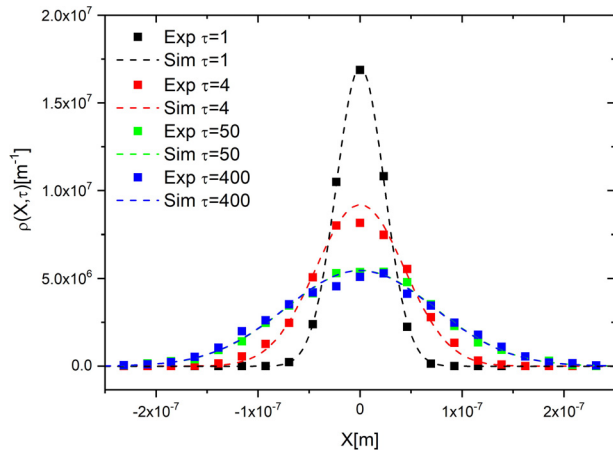


Fig. 7. Comparison of the probability function $\rho(x, t)$ for particles trapped in a parabolic potential and the BD simulation at four lag times: $\tau = 1, 4, 50,$ and 400 , with $\tau = t/(100 \text{ ms})$, at a laser power of 6 mW .

nowadays accessible not only to graduate but also to undergraduate students, and the data analysis is relatively straightforward given the recent advances in tracking techniques. We have shown that the theoretical framework used to describe the phenomena can be quantitatively compared with experimental results, and that Brownian dynamics simulations are easy to implement, even for non-specialists. The authors hope that this contribution provides a useful insight on optical tweezers, both from a teaching perspective, but also as a starting point for scientific applications, and that it could serve as a practical guide to understand the optical trapping of colloidal particles from an experimental and simulation point of view.

ACKNOWLEDGMENTS

E.S.-G. acknowledges CONAHCYT Mexico through Grant No. A1-S-9098 and grant Ciencia de Frontera 102986. B.M.-C. acknowledges CONAHCYT Mexico through Grant No. A1-S-9887. G.I. G.-G. acknowledges the SEP-CONACYT CB-2016 Grant No. 286105, the 2019 Marcos Moshinsky Fellowship, and the National Supercomputing Center-IPICYT for the computational resources supported in this research through the Grant No. TKII-IVGU001, as well as the computing time granted by LANCAD and CONAHCYT on the supercomputer Yoltla/Miztli/Xiuhcoatl at LSVP UAM-Iztapalapa/DGTIC UNAM/CGSTIC CINVESTAV with the Project No. 58-2021. G.I.G.-G. also expresses his gratitude for the assistance from the computer technicians at the IF-UASLP.

AUTHOR DECLARATIONS

Conflict of Interest

The authors have no conflicts to disclose.

APPENDIX: ONE-DIMENSIONAL BROWNIAN DYNAMICS WITH EXTERNAL FORCE PSEUDO-CODE

Set the initial position of the particle, e.g., $x_{old} = 0$, and initialize the values of D, a, k or α (see the text), and dt .

DO $i = 1$ up to max_{steps}

Calculate $x_{new} = x_{old} + \frac{D}{k_B T} F(x_{old}, k) dt + \sqrt{2Ddt} G_i$

where $F(x_{old}, k) = -kx_{old} = -\frac{2ak_B T}{a^2} x_{old}$, and

G_i corresponds to a random number obtained from a normal distribution with mean $\mu = 0$ and variance $\sigma = 1$. This random number can be obtained, e.g., via the Box–Mueller algorithm³⁹ or from an equivalent available implementation in a chosen programming language.

Record x_{new}

$i = i + 1$

$x_{old} = x_{new}$

END DO

^{a)}ORCID: 0000-0002-5977-2633.

^{b)}ORCID: 0000-0003-1144-657X.

^{c)}ORCID: 0000-0002-3174-2643.

^{d)}Author to whom correspondence should be addressed: esarmiento@fisica.ugto.mx, ORCID: 0000-0001-6130-4161.

¹J. K. G. Dhont, *An Introduction to Dynamics of Colloids* (Elsevier Science, Amsterdam, 1996).

²R. Brown, “XXVII. A brief account of microscopical observations made in the months of June, July and August 1827, on the particles contained in the pollen of plants; and on the general existence of active molecules in organic and inorganic bodies,” *Philos. Mag.* **4**(21), 161–173 (1828).

³V. V. Raman, “Jean Baptiste Perrin: Advocate for the atoms?,” *Phys. Teach.* **8**(7), 380–386 (1970).

⁴D. L. Ermak and J. A. McCammon, “Brownian dynamics with hydrodynamic interactions,” *J. Chem. Phys.* **69**(4), 1352–1360 (1978).

⁵P. Haldas and E. R. Weeks, “Video microscopy of colloidal suspensions and colloidal crystals,” *Curr. Opinion Colloid Interface Sci.* **7**(3–4), 196–203 (2002).

⁶G. E. Uhlenbeck and L. S. Ornstein, “On the Theory of the Brownian Motion,” *Phys. Rev.* **36**(5), 823–841 (1930).

⁷W. M. Lee, P. J. Reece, R. F. Marchington, N. K. Metzger, and K. Dholakia, “Construction and calibration of an optical trap on a fluorescence optical microscope,” *Nat. Protoc.* **2**(12), 3226–3238 (2007).

⁸P. H. Jones, O. M. Maragó, and G. Volpe, *Optical Tweezers: Principles and Applications* (Cambridge U. P., Cambridge, 2015), pp. 188–217.

⁹G. Volpe and G. Volpe, “Simulation of a Brownian particle in an optical trap,” *Am. J. Phys.* **81**(3), 224–230 (2013).

¹⁰Thorlabs, see https://www.thorlabs.com/newgrouppage9.cfm?object_group_id=3959 for “Modular optical tweezers” (2023) (accessed October 19, 2023).

¹¹M. C. Wang and G. E. Uhlenbeck, “On the Theory of the Brownian Motion II,” *Rev. Mod. Phys.* **17**(2–3), 323–342 (1945).

¹²A. Einstein, “Über die von der molekularinetischen Theorie der Wärme geforderte Bewegung von in ruhenden Flüssigkeiten suspendierten Teilchen,” *Ann. Phys.* **322**, 549–560 (1905).

¹³H. Löwen, “Colloidal soft matter under external control,” *J. Phys.: Condens. Matter* **13**(24), R415–R432 (2021).

¹⁴M. C. Jenkins and S. U. Egelhaaf, “Colloidal suspensions in modulated light fields,” *J. Phys.: Condens. Matter* **20**(40), 404220 (2008).

¹⁵Masao Doi and S. F. Edwards, “Dynamics of concentrated polymer systems. Part 2.—Molecular motion under flow,” *J. Chem. Soc., Faraday Trans. 2* **74**(0), 1802–1817 (1978).

¹⁶R. F. Fox and G. E. Uhlenbeck, “Contributions to non-equilibrium thermodynamics. I. Theory of hydrodynamical fluctuations,” *Phys. Fluids* **13**(8), 1893–1902 (1970).

¹⁷G. L. Hunter and E. R. Weeks, “The physics of the colloidal glass transition,” *Rep. Prog. Phys.* **75**(6), 066501 (2012).

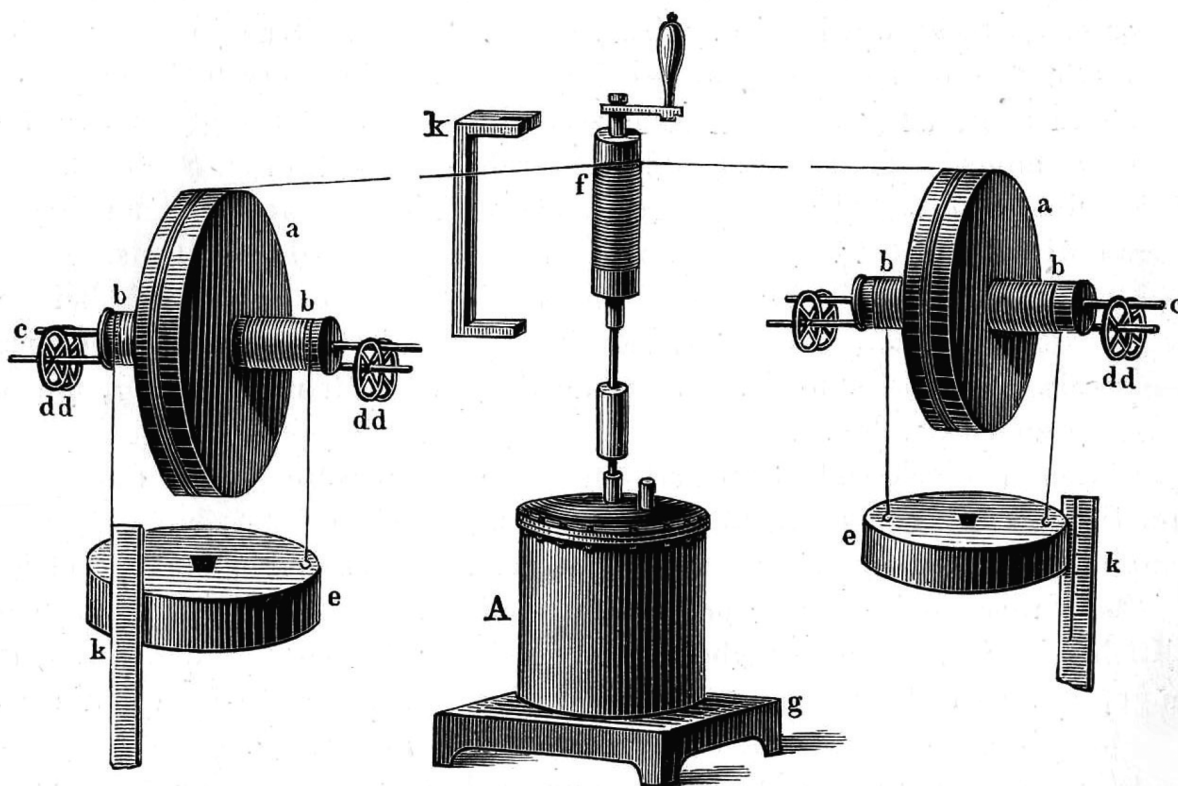
¹⁸U. Seifert, “Stochastic thermodynamics, fluctuation theorems and molecular machines,” *Rep. Prog. Phys.* **75**(12), 126001–126058 (2012).

¹⁹Rongxin Huang, Isaac Chavez, Katja M. Taute, Branimir Lukić, Sylvia Jeney, Mark G. Raizen, and Ernst-Ludwig Florin, “Direct observation of the full transition from ballistic to diffusive Brownian motion in a liquid,” *Nat. Phys.* **7**(7), 576–580 (2011).

²⁰R. Kubo, “The fluctuation-dissipation theorem,” *Rep. Prog. Phys.* **29**(1), 255–284 (1966).

²¹G. Pesce, G. Volpe, O. M. Maragó, P. H. Jones, S. Gigan, A. Sasso, and G. Volpe, “Step-by-step guide to the realization of advanced optical tweezers,” *J. Opt. Soc. Am. B* **32**(5), B84–B98 (2015).

- ²²X. Bian, C. Kim, and G. E. Karniadakis, "111 years of Brownian motion," *Soft Matter* **12**(30), 6331–6346 (2016).
- ²³J. C. Crocker and D. G. Grier, "Methods of digital video microscopy for colloidal studies," *J. Colloid Interface Sci.* **179**(1), 298–310 (1996).
- ²⁴D. L. Ermak, "A computer simulation of charged particles in solution. I. Technique and equilibrium properties," *J. Chem. Phys.* **62**(10), 4189–4196 (1975).
- ²⁵M. P. Allen and D. J. Tildesley, *Computer Simulation of Liquids* (Clarendon Press, Oxford, 1989).
- ²⁶D. B. Allan, T. Caswell, N. C. Keim, C. M. van der Wel, and R. W. Verweij (2023). "soft-matter/trackpy: v0.6.1," Zenodo. <https://doi.org/10.5281/zenodo.7670439>
- ²⁷J. Bewerunge, I. Ladadwa, F. Platten, C. Zunke, A. Heuer, and S. U. Egelhaaf, "Time- and ensemble-averages in evolving systems: The case of Brownian particles in random potentials," *Phys. Chem. Chem. Phys.* **18**(28), 18887–18895 (2016).
- ²⁸A. Lubelski, I. M. Sokolov, and J. Klafter, "Onergodicity mimics inhomogeneity in single particle tracking," *Phys. Rev. Lett.* **100**(25), 250602 (2008).
- ²⁹A. Ashkin and J. M. Dziedzic, "Optical levitation by radiation pressure," *Appl. Phys. Lett.* **19**(8), 283–285 (1971).
- ³⁰A. Ashkin, "Optical trapping and manipulation of neutral particles using lasers," *Proc. Natl. Acad. Sci. U. S. A.* **94**(10), 4853–4860 (1977).
- ³¹A. Ashkin, J. M. Dziedzic, J. E. Bjorkholm, and S. Chu, "Observation of a single-beam gradient force optical trap for dielectric particles," *Opt. Lett.* **11**(5), 288–290 (1986).
- ³²J. E. Molloy and M. J. Padgett, "Lights, action: Optical tweezers," *Contemp. Phys.* **43**(4), 241–258 (2002).
- ³³A. Ashkin, "History of optical trapping and manipulation of small-neutral particle, atoms, and molecules," *IEEE J. Select. Top. Quantum Electron.* **6**(6), 841–856 (2000).
- ³⁴J. R. Moffitt, Y. R. Chemla, S. B. Smith, and C. Bustamante, "Recent advances in optical tweezers," *Annu. Rev. Biochem.* **77**(1), 205–228 (2008).
- ³⁵D. G. Grier, "Optical tweezers in colloid and interface science," *Curr. Opin. Colloid Interface Sci.* **2**(3), 264–270 (1997).
- ³⁶M. X. Fernandes and J. G. de la Torre, "Brownian dynamics simulation of rigid particles of arbitrary shape in external fields," *Biophys. J.* **83**(6), 3039–3048 (2002).
- ³⁷L. J. Hou, Z. L. Mišković, A. Piel, and P. K. Shukla, "Brownian dynamics simulation of rigid particles of arbitrary shape in external fields," *Phys. Plasmas* **16**(5), 053705 (2009).
- ³⁸A. Razali, C. J. Fullerton, F. Turci, J. E. Hallett, R. L. Jack, and C. P. Royall, "Effects of vertical confinement on gelation and sedimentation of colloids," *Soft Matter* **13**(17), 3230–3239 (2017).
- ³⁹G. E. P. Box and M. E. Muller, "A note on the generation of random normal deviates," *Ann. Math. Stat.* **29**(2), 610–611 (1958).
- ⁴⁰A guideline installation and example codes can be found on the developer's web page, <https://soft-matter.github.io/trackpy/v0.6.1/>.



Joule's Mechanical Equivalent of Heat Apparatus

The heart of the apparatus is contained in the cylinder at the bottom center. Here perforated rotating blades stir the water; as mechanical work is done on the water its temperature increases. The work is done by the two falling bodies on each side. The original figure is from an 1872 paper by James Prescott Joule. From: Müller-Pouillet. *Lehrbuch der Physik* (Braunschweig, 1907) pg 622. (Picture and text by Thomas B. Greenslade, Jr., Kenyon College)